FEATURE ARTICLE

Nanocrystal and Nanowire Synthesis and Dispersibility in Supercritical Fluids

Parag S. Shah, Tobias Hanrath, Keith P. Johnston,* and Brian A. Korgel*

Department of Chemical Engineering, Texas Materials Institute, and Center for Nano- and Molecular Science and Technology, The University of Texas at Austin, Austin, Texas 78712

Received: January 13, 2004; In Final Form: March 6, 2004

Here we review major breakthroughs in the rapidly developing research area of nanomaterial synthesis in supercritical fluids focusing on both the fundamental science and processing advantages in the application areas of separations, assembly and scale-up of synthesis. Density-tunable control of the solvation strength, along with favorable interfacial tensions, wetting, and transport properties make supercritical fluids (SCFs) unique and potentially superior solvent media for the synthesis and processing of nanoscale metals and semiconductors. The steric repulsion between particle cores may be tuned by adjusting the solvent density to control the nanocrystal size and polydispersity during single-phase synthesis, and to achieve size-selective nanocrystal precipitation. Compressed solvents at the vapor pressure can also be used to deposit nanocrystal monolayers at controlled evaporation rates without dewetting at higher rates than conventional solvents. The high synthetic temperatures accessible in SCFs can be used to promote the crystallization of covalent nanomaterials, while maintaining a reaction environment capable of solvating reactants and capping ligands. This allows semiconductor nanocrystals exhibiting size-dependent photoluminescence to be synthesized at temperatures well above the boiling point of conventional solvents. Finally, gold nanocrystal seed particles can be used to synthesize bulk quantities of defect-free silicon and germanium nanowires, several micrometers in length.

I. Introduction

Various metal and semiconductor nanocrystals and nanowires have been produced by solution-phase colloidal synthetic routes to achieve controlled size, size distribution, and chemical stability. These materials have been used to experimentally examine size-dependent quantum mechanical and physical chemical phenomena[1−3] and, in recent years, have been merged with structures fabricated using top-down patterning, deposition and etching techniques to produce a variety of prototype optical and electronic devices, such as light emitting diodes and transistors.[4−9] Ultimately, a "hybrid" device fabrication approach could lead to a variety of applications, ranging from flat panel displays, solid-state lighting, flash memory, multivalue logic, sensing, and on-chip therapeutic medical technologies. For these applications to become a commercial reality, many improvements in materials synthesis, processing, and properties are still required, and the ability to deposit and self-assemble nanocrystals and nanowires accurately and efficiently still presents a major fundamental hurdle. Nonetheless, the chemical, solution-phase approach to nanocrystal and nanowire synthesis has played an important role in developing our understanding of fundamental nanostructure physical properties and can be expected to play an increasingly fundamental role in the creation of future nanotechnologies.

Colloidal size stabilization can be accomplished by two different approaches: (1) compartmentalized or templated growth and (2) arrested precipitation. Compartmentalized growth has been explored in a variety of media, including liposomes, porous glasses, polymer matrices, and zeolites, and these methods have been reasonably successful in controlling size.[10] However, applications usually require the template to be removed, which leads to immediate deterioration of the size distribution and flocculation of the nanocrystals. Surfactants that bind to the nanocrystal surface, called "capping ligands", can be added to provide a "soft" sterically repulsive layer that chemically passivates the surface and provides colloid stability. The nanocrystals can also be synthesized directly in the presence of capping ligands, through a process called arrested precipitation. Arrested precipitation has been very successful in producing sterically stabilized nanocrystals of a wide range of chemistries, including groups II−VI, III−V, and IV semiconductors, as well as various metals and oxides.[3,11−14] Often the nanocrystal size distribution is narrowed by size-selective precipitation with the addition of an antisolvent. The capping ligand chemistry can also be made chemically functional for selective binding to recognition molecules or substrates. In the past few years, researchers have been exploring the potential of using different capping ligand chemistry to control nanocrystal shape. This approach has yielded nanorods of various materials, including CdSe[15] and Co.[16] A more rational approach to shape control and rod/wire production involves the use of metal nanocrystal seeds that direct the formation of semiconductor nanowires that have been used to synthesize high-quality nanorods and nanowires in solution.[17−19] Solution-phase routes

* Corresponding authors. K.P.J.: e-mail, kpj@che.utexas.edu; tel, 512-471-4617; fax, 512-471-7060. B.A.K.: e-mail, korgel@che.utexas.edu; tel, 512-471-5633; fax, 512-471-7060.

10.1021/jp049827w CCC: $27.50
Published on Web 06/11/2004

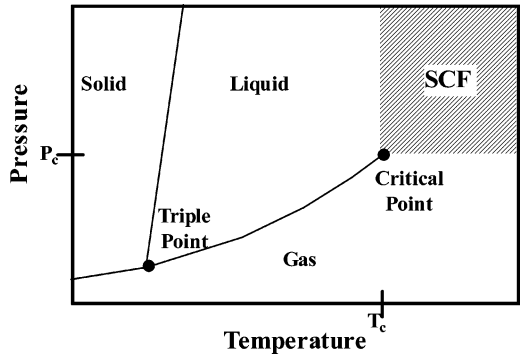

Figure 1. Schematic of pressure−temperature phase diagram showing the triple point, the critical point and the supercritical region.

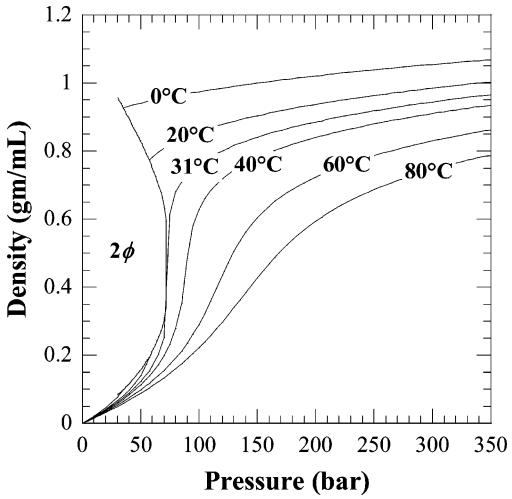

Figure 2. Carbon dioxide density as a function of pressure and temperature.

TABLE 1: Physical Properties of a Supercritical Fluid Fall between Those of a Typical Gas and Liquid

	liquid	supercritical fluid	gas
density (g/mL)	1	0.05−1	10^{-3}
viscosity (Pa·s)	10^{-3}	10^{-4} to 10^{-5}	10^{-5}
diffusion coefficients (cm^2/s)	10^{-5}	10^{-3}	10^{-1}
surface tension (mN/m)	20−50	0	0

to nanomaterials can provide control over size, shape, and surface chemistry.

During the past few years, our research groups and others have been exploring the use of solvents heated and pressurized above their critical points—called supercritical fluids (SCFs)—for nanocrystal and nanowire synthesis, stabilization, and processing. Although conventional solvents provide a flexible medium for nanocrystal synthesis, supercritical fluids exhibit some unique properties that have significant utility when applied to these chemical systems. At temperatures and pressures beyond the critical point in the vapor−liquid coexistence curve (at $T > T_c$ and $P > P_c$), only a single-phase fluid exists as shown schematically in Figure 1. In this single-phase region of the phase diagram, the density, viscosity, and diffusivity are intermediate between those of liquids and gases, as shown in Table 1, and vary continuously from gaslike to liquidlike with modest changes in temperature and pressure.[20] The solvent strength, which relates to solvent density, can be tuned by varying the pressure or temperature as illustrated in the CO_2 phase diagram in Figure 2. Continuous solvent strength tunability with slight pressure and/or temperature changes can be useful for manipulating the solvation of steric stabilizers and thus colloidal stability. A variety of colloids have been stabilized in SCF CO_2 and in high-temperature supercritical fluids, as shown in Table 2. One of the factors that enabled nanocrystal and nanowire chemistry in SCFs was the discovery of low molar mass steric stabilizers for colloids in supercritical fluid hydrocarbons and in carbon dioxide (Table 2). For example, fluoroalkane and oligomeric perfluoropolypropylene oxide groups utilized in surfactant tails designed for water-in-carbon dioxide microemulsions[21−24] were also successful for the stabilization of metal nanocrystals in CO_2.[25−27] The tunability of SCFs may be used to achieve size control during arrested precipitation nanocrystal synthesis[28] and size-selective precipitation that does not require the addition of an antisolvent.[29] The intermediate transport properties of SCFs allow faster rates in diffusion-limited reactions compared to liquid systems.[30] The high densities provide solvation and thus increased reactant loadings compared to gas-phase systems.[31,32] SCFs are well suited for particle deposition and assembly on surfaces[33] and within porous materials due to their unique wetting properties.[34,35] The single-phase fluids do not exhibit a liquid−vapor interface, thereby eliminating surface tension driven Laplace pressures, which would otherwise collapse porous structures during solvent removal. Even subcritical fluids such as liquid CO_2 can have interfacial tensions that are much lower than conventional solvents. SCF solvents also provide access to high temperatures (350−600 °C) that are well above the boiling points of conventional solvents under ambient pressures—a key characteristic that enables access to synthetic temperatures needed to crystallize highly covalent nanocrystals, such as Si[13] and Ge,[36] and for the general application of the metal particle-seeded VLS-type growth of nanowires in solution.[19,37−39] Furthermore, the use of supercritical CO_2 can provide an environmentally sound alternative to conventional solvents used for nanocrystal and nanowire synthesis and processing.

Here we review the rapid progress made during the course of the past few years in the use of SCF solvents for nanocrystal and nanowire synthesis, stabilization, and processing, with particular emphasis on our current understanding of the potential applications and future limitations of SCF solvents for these processes.

II. Colloid Stabilization in Supercritical Fluids

The design of ligands for nanocrystal dispersibility and synthesis in SCFs has been aided by an emerging fundamental understanding of colloid stability in compressible solvents. Highly compressible SCFs gain considerable entropy upon expanding away from solutes during phase separation and likewise during flocculation of colloids, an effect not present in conventional, relatively incompressible, liquid solvents such as alkanes. Whereas conventional solvents often exhibit upper critical solution temperature (UCST) phase behavior, where phase separation is enthalpically driven, SCFs typically exhibit entropically driven lower critical solution temperature (LCST) phase behavior in which an increase in temperature at constant pressure lowers solubility.[40] Analogously, this LCST-type phase separation may also be produced by a decrease in pressure (and likewise solvent density) at constant temperature at the upper critical solution density (UCSD).[41]

To describe colloid stability in compressible SCFs, Peck[42] combined self-consistent field theory with lattice fluid theory (LFSCF) to model the structure and interactions between short terminally attached chains. Meredith extended the theory to treat high molecular weight chains,[43] and also utilized Monte Carlo simulation to determine the structure and interactions of end-

TABLE 2: Key Advances in Supercritical Fluid Based Colloidal Dispersions

colloid and supercritical fluid	stabilizing group
water-in-alkane microemulsion (1988)	alkane[122]
water-in-CO_2 microemulsion (1994)	a. alkane/fluoroalkane hybrid[21,22]
	b. perfluoropolypropylene oxide (<1000 molar mass)[23,24]
polymer latex in CO_2 (1994)	polymeric flouroacrylates and siloxanes (high molar mass)[53]
metal and semiconductor nanocrystals in water/CO_2 microemulsion (1999)	a. perfluoropolypropylene oxide and alkane[25]
	b. perfluoropolypropylene oxide[26]
metal nanoparticle dispersion in water (2000)	a. without stabilizer[106]
	b. alkanethiols[14]
metal nanocrystal dispersion in CO_2 (2000)	fluoroalkanethiol[27]
gold nanocrystals for synthesis of Si nanowires in alkanes and octanol at high temperature (2000)	alkanethiol[19]
Si nanocrystal dispersion in alkanes and octanol (high *T*) (2001)	octanol[13]

grafted chains with 20 to 60 segments in a compressible solvent.[44] In each case lowering the solvent density collapses the chains as the solvent gains entropy by expanding away from the chains and into bulk solution. Furthermore, a critical flocculation density (CFD) was identified where the attractive interaction between two coated surfaces becomes greater than the thermal energy, $^3/_2kT$, in the absence of core−core attraction. The CFD was found to correspond to the upper critical solution density (UCSD) of the chains in bulk solvent. Complementary experimental studies have examined the relationship between the stabilizer phase behavior and the critical flocculation density for organic-in-CO_2 emulsions,[45] water-in-CO_2 emulsions[46] and silica colloids sterically stabilized in supercritical CO_2 by end-grafted polymers.[47,48] In addition, the conformation of grafted chains on surfaces in SCFs has been measured with neutron reflectivity.[49] The interactions between the grafted chains and between the grafted chains and surfaces, relative to the weak interactions between the chains and CO_2 produce larger effects of solvent quality on polymer conformation than for liquid solvents. The design of successful ligands for nanocrystal dispersions must take into account these large asymmetries and the large compressibility, especially for CO_2, a particularly weak solvent.

CO_2 has received significant attention among SCFs because it is nonflammable, essentially nontoxic and environmentally benign. Its low critical temperature and pressure of 31 °C and 71 bar are easily accessible. However, CO_2's low polarizability per volume (and refractive index) result in far weaker van der Waals forces than in the case of hydrocarbon solvents, making it more like a fluorocarbon.[41,50−52] Because of CO_2's unusual solvation properties and high compressibility, novel "CO_2-philic" ligands are required to sterically stabilize colloids in CO_2. High molecular weight stabilizers based on fluoropolymers and siloxanes have been developed for kinetically stable dispersions including polymer latexes[53,54] and water-in-CO_2 (W/C) emulsions.[55] In contrast, low molecular weight fluoroalkane,[21,22] fluoroether,[23] and branched hydrocarbon surfactants have been designed to form reverse micelles in CO_2[56] as well as thermodynamically stable W/C microemulsions.[57] Small angle neutron scattering (SANS) studies on fluoroether stabilized W/C microemulsion have shown that the weak solvation of the surfactant tails by CO_2 results in stronger tail−tail interactions compared with water/alkane microemulsions stabilized with conventional hydrocarbon surfactants.[58] Decreasing the solvent density weakens tail solvation and increases tail−tail interactions further. This limited solvation has been a major challenge in designing stabilizers for microemulsions as well as nanocrystal dispersions in CO_2. However, surfactant tails or ligands with low interfacial free volume reduce the overlap between the tails and provide a stronger barrier to flocculation.[59]

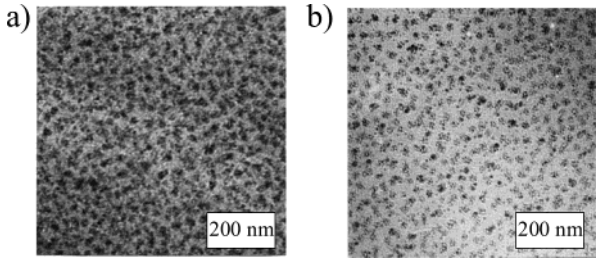

Figure 3. TEM micrographs of silver deposited within copolymer of PS-*b*-PAA: (a) unreduced silver precursor selectively bound within blocks of PAA; (b) reduction yields silver clusters within the PAA domains. Reproduced with permission from Brown et al. (*Polym. Mater. Sci. Eng.* **2000**, *82*, 292−293). Copyright 2000 American Chemical Society.

III. Approaches to Nanoparticle Formation Using Supercritical Solvents

Chemical Fluid Deposition (CFD). Watkins and co-workers demonstrated one of the earliest examples of nanoparticle formation in a supercritical fluid in 1995 by forming Pt nanoparticles on a polymer substrate immersed in supercritical CO_2 through the reduction of CO_2-soluble organometallic precursors using hydrogen.[60] CO_2 allowed for very high solubility of the gas reductant H_2 as well as much higher loadings of the organometallic precursor relative to chemical vapor deposition (CVD) systems. They later demonstrated selective metal deposition in one of the phases of a block copolymer substrate resulting in the templated synthesis of nanoparticles as shown in Figure 3.[61,62] Watkins and co-workers later used this technique, chemical fluid deposition (CFD), to deposit conformal metal films onto various substrates. The CFD process yielded copper films with fewer defects than those possible using CVD as a result of increased precursor solubility while at the same time allowing effective filling of high aspect ratio voids due to the lack of wettability constraints prevalent in conventional solvents.[35,63]

Water-in-CO_2 (W/C) Microemulsions. Water-in-CO_2 (W/C) microemulsions have been exploited for the solution-phase synthesis of metallic and semiconductor nanoparticles. Surfactant-stabilized aqueous cores dispersed in a continuous CO_2 phase provide a convenient medium for exploring nanocrystal synthesis in supercritical solvents. The formation of water-in-CO_2 microemulsions requires an understanding of interfacial curvature and droplet interactions, all of which are active areas of research.[64−66] For microemulsions with water cores, the surfactant geometry must cause the interface to curve around water and the surfactant tails must be adequately solvated by the SCF environment. Thermodynamic models for the properties of microemulsions in supercritical fluids, including the curvature, water uptake, bending moment and droplet attraction have been developed.[67] The nanometer-size aqueous cores of the micelles

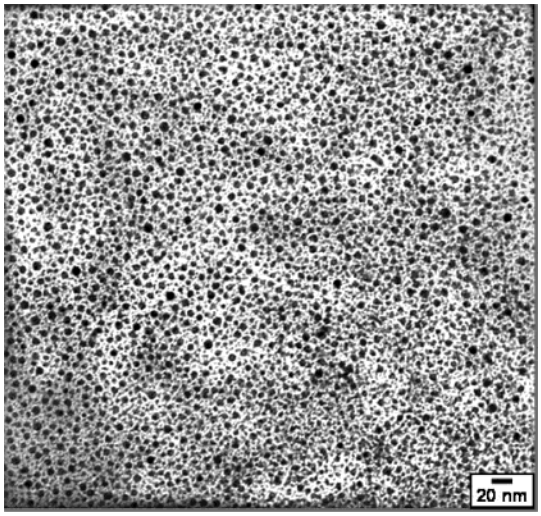

Figure 4. Copper nanocrystals synthesized in propane/AOT reverse micelle system at 241 bar and 21 °C capped with dodecanethiol. Reproduced with permission from Kitchens et al. (*Ind. Eng. Chem. Res.*, submitted for publication).

provide solubility of metal salts (that are insoluble in CO_2) and can serve as nanoreactors that compartmentalize precipitation. Although the micelles rapidly exchange material and do not serve as a truly compartmentalized media for growth, the surfactant limits particle size by weakly adsorbing to the surface of the growing particles, allowing the particle size to be roughly tuned through the micelle size. Using this approach, research groups have synthesized silver,[25,68,69] copper,[68] silver halide,[70] CdS,[26,71] and ZnS[71] in W/C microemulsions. A detailed study done by Cason and Roberts on the synthesis of copper nanoparticles in sc-ethane- and sc-propane-based microemulsions showed that greater interactions between micelles in SCFs led to faster growth rates compared to conventional solvents.[72−74] In addition, increasing the water content led to a faster reaction. Recently, Kitchens and Roberts showed that the density-tunable solvation strength impacts the final particle size for Cu nanocrystals synthesized in ethane- and propane-based reverse micelles, with lower density leading to smaller particle size (Figure 4).[75,76] In the case of silver nanocrystals in W/C microemulsions, it was found that at short times numerous intermediate species were formed that were interacting with the ammonium headgroup of the surfactant.[69] Holmes et al. synthesized semiconductor nanoparticles of cadmium sulfide, in PFPE $COO^-NH_4^+$ stabilized W/C microemulsions.[26] In this case the particle radii of approximately 9 and 18 Å, respectively, were consistent with the microemulsion droplet diameters determined from SANS. In contrast to the other microemulsion-based systems, here the binding of the surfactant molecules to the particle surface was sufficient to enable the particles to be collected and redispersed in ethanol without coalescence.

Rapid Expansion from Supercritical Solution (RESS). Sun et al. have synthesized various materials using RESS, including Ni,[77] Co,[77] Pt,[77] PbS,[78] and CdS.[79] In this process, a precursor is dissolved in a hot SCF solution and expanded into a room temperature solvent such as ethanol through a nozzle. The SCF was typically an organic solvent, e.g., ammonia, heated to over 100 °C, which was expanded into room temperature water or ethanol containing reducing agents and a stabilizing polymer, usually poly(vinylpyridine) (PVP), which adsorbs to the nanocrystal surface to prevent coalescence. The particle size and polydispersity could be roughly controlled by tuning the pressure drop across the nozzle, as well as the nozzle geometry itself. W/C microemulsions containing dissolved silver salts have also been expanded into a solution of reducing agent and PVP to form metal particles.[80] This technique eliminates the need for harsh organic solvents.

Precipitation with a Compressed Antisolvent(PCA). Alternatively, an organic solvent can be sprayed into CO_2, which serves as an antisolvent that generates particle formation[81−84] The rapid two-way mass transfer of organic solvent into CO_2 and vice versa can rapidly supersaturate the solvent. This antisolvent process was used by Gupta et al. to precipitate particles of agglomerated fullerenes (C_{60}), which were as small as 29 nm, compared to 40 μm using conventional solvents.[85]

IV. Arrested Precipitation and Steric Stabilization in Supercritical Fluids

Arrested precipitation has been one of the most successful synthetic approaches in conventional solvents for a variety of different nanocrystals.[3,12] The nanocrystals are synthesized in the presence of a capping ligand, which binds to the particle surface and quenches growth, while at the same time controlling dispersibility and dispersion stability. A significant amount of recent research has focused on understanding nanocrystal steric stabilization in supercritical solvents,[27,29] as it is central to both synthetic control and processing capabilities. The sterically stabilized nanocrystals can be collected, purified, and size-selected, by precipitation, and then redispersed in either a conventional or SCF solvent for deposition onto substrates.

Nanocrystal Dispersibility in Supercritical Fluids. Nanocrystal dispersion stability is determined by the balance between attractive core−core van der Waals interactions and repulsive steric interactions between adsorbed ligand chains. The van der Waals interactions are the macroscopic result of dipole−induced dipole interactions and depend on the physical properties of the particles and the dispersing medium.[86,87] For like materials, the van der Waals force is always attractive—the interparticle potential is *negative*—and depends on the particle diameter D, the center-to-center separation distance d and the Hamaker constant, A_{131}:

$$\Phi_{vdW} = -\frac{A_{131}}{6}\left[\frac{D^2}{2d^2 - 2D^2} + \frac{D^2}{2d^2} + \ln\left(\frac{d^2 - D^2}{d^2}\right)\right] \quad (1)$$

The van der Waals attraction increases with an increase in particle size and decrease in separation distance. The Hamaker constant, A_{131}, for particles composed of material "1" interacting across a medium of material "3" depends on the difference in dielectric constants ϵ, and refractive indices n, and can be estimated using a simplification developed by Lifshitz,[86,87]

$$A_{131} = \frac{3}{4}k_b T\left(\frac{\epsilon_1 - \epsilon_3}{\epsilon_1 + \epsilon_3}\right)^2 + \frac{3h\upsilon_e\,(n_1^2 - n_3^2)^2}{16\sqrt{2}(n_1^2 + n_3^2)^{3/2}} \quad (2)$$

where h is Planck's constant, k_b is Boltzmann's constant, T is temperature, and υ_e is the maximum electronic ultraviolet adsorption frequency, typically taken to be 3×10^{15} s^{-1}. In SCFs, both the dielectric constant and refractive index are relatively strong functions of temperature and pressure,[88] and must be accounted for in Hamaker constant calculations relevant to nanocrystal dispersions.[28,29]

The adsorbed ligands provide a steric repulsive layer that counterbalances the core-core van der Waals attraction between particles. As two nanocrystals approach each other, their

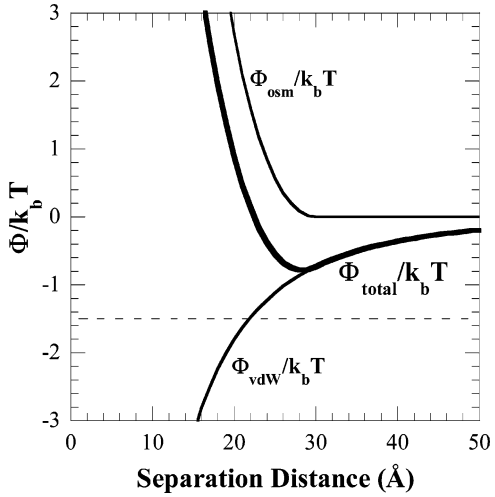

Figure 5. Total interaction potential (Φ_{total}) between silver nanocrystals in sc-ethane at 35 °C and 276 bar. Adapted with permission from Shah et al. (*J. Phys. Chem. B* **2002**, *106*, 2545−2551). Copyright 2002 American Chemical Society.

stabilizing ligands begin to overlap and give rise to an osmotic repulsion (Φ_{osm}):[89,90]

$$\Phi_{osm} = \frac{2\pi D k_b T}{v_{solv}} \phi^2 \left(\frac{1}{2} - \chi\right)\left(l - \frac{d-D}{2}\right)^2 \qquad l < d - D < 2l \tag{3}$$

$$\Phi_{osm} = \frac{2\pi D k_b T}{v_{solv}} \phi^2 \left(\frac{1}{2} - \chi\right)\left[l^2\left(\frac{d-D}{2l} - \frac{1}{4} - \ln\left(\frac{d-D}{l}\right)\right)\right] \qquad d - D < l \tag{4}$$

Φ_{osm} depends on the molecular volume of the solvent v_{solv}, the volume fraction profile of the ligand extending from the particle surface ϕ, ligand length l, and the Flory−Huggins interaction parameter χ, which indicates the solvent−ligand compatibility. $\chi = {}^1/_2$ represents the boundary between a good solvent ($\chi < {}^1/_2$) and poor solvent ($\chi > {}^1/_2$). Most good solvents for alkanethiol-coated nanocrystals, such as hexane or chloroform, have χ parameters close to zero. Notice that $\Phi_{osm} < 0$ in poor solvents indicating attractive interactions between the ligands due to inadequate tail solvation.

The stability of a colloidal dispersion can be estimated by summing the interparticle interactions: $\Phi_{total} = \Phi_{vdW} + \Phi_{osm}$. Figure 5 provides an example of such a calculation. A dispersion with an attractive well lower than $-{}^3/_2 k_b T$ is unstable and prone to flocculation. In SCFs, χ can be tuned continuously with temperature and pressure changes and must be adequately low (i.e., high density) for significant repulsive interactions to occur between capping ligands. The Hamaker constant is also a function of solvent density in SCFs and increases with decreasing density, compounding the challenges to nanocrystal stabilization in SCFs at lower density.

Density-Dependent Dispersibility in Supercritical Ethane. Dodecanethiol-coated silver and gold nanocrystals in sc-ethane represent a powerful model system to test the fundamental ideas presented above for steric stabilization in supercritical solvents.[29,91] Alkanethiol-stabilized nanocrystals can be synthesized using standard two-phase arrested precipitation techniques, purified, and then transferred to a high-pressure cell to follow the density-dependent dispersibility by UV−visible absorbance spectroscopy. Figure 6 shows the characteristic plasmon peak for silver nanocrystals dispersed in ethane at 35 °C. The plasmon peak extinction coefficient decreases with decreased pressure

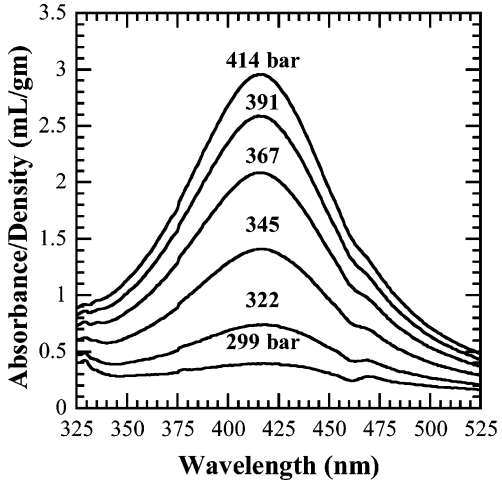

Figure 6. Silver nanocrystal absorbance in supercritical ethane at 35 °C and various pressures. Reproduced with permission from Shah et al. (*J. Phys. Chem. B* **2002**, *106*, 2545−2551). Copyright 2002 American Chemical Society.

as nanocrystals settle out of solution due to reduced dispersibility. This same trend in pressure-dependent dispersibility has been observed at 45 °C. At a constant pressure of 414 bar, increasing temperature from 25 to 55 °C also decreases the nanocrystal dispersibility. To test the size-dependence of the dispersibility, a bimodal sample of gold nanocrystals (18 and 42 Å in diameter) in ethane has been followed with absorbance spectroscopy at various solvent densities. Smaller gold nanocrystals (18 Å) could be dispersed at 138 bar, whereas the larger gold particles (42 Å) required pressures up to 414 bar, at 25 °C. Size-dependent dispersibility, as evidenced spectroscopically by the gold nanocrystals, was observed for silver nanocrystals by TEM imaging of samples collected from ethane dispersions at 35 °C and 414 and 317 bar.[29] Size determination by TEM revealed that the average particle size and polydispersity dropped with decreased solvent density at 35 °C, with $D = 53 \pm 19$ Å for the original sample, $D = 37 \pm 18$ Å at 414 bar, and $D = 24 \pm 13$ Å at 317 bar. Dodecanethiol-coated nanocrystals larger than approximately 40 Å in radius could not be dispersed at 414 bar, and nanocrystals larger than ∼60 Å in diameter would not disperse at 317 bar. The precipitation and redispersion of the silver nanocrystals was found to be nearly reversible. Increasing the system pressure could redisperse approximately 90% of the nanocrystals precipitated by the lowering solvent density, allowing for reversible solvation, which is difficult to achieve using conventional antisolvent-based approaches where solvation strength is extremely sensitive to the antisolvent concentration and antisolvent cannot easily be removed. This same size-dependent dispersibility trend was observed by Clarke et al.,[91] where they showed that although they could not achieve sufficiently high densities to disperse larger nanocrystals ($D =$ 50 Å), small gold nanocrystals ($D = 17$ Å) could be dispersed at low ethane pressures.

Shah et al.[29] found that the density-dependent nanocrystal dispersibility could be predicted reasonably well using the model equations presented above, by calculating the difference in the Hildebrand solubility parameter δ_i (or the cohesive energy density, $c_i = \delta_i^2$) of the ligand ($i = 2$) and the solvent ($i = 1$) to determine density-dependent χ parameters.

$$\chi = \frac{v_i}{RT}(\delta_1 - \delta_2)^2 \tag{5}$$

Here, v_i is the molar volume and the cohesive energy density

of the solute and solvent is given by

$$c_i = \delta_i^2 = \frac{h_{i,\mathrm{ig}} - RT - h_i + P\upsilon_i}{\upsilon_i} \quad (6)$$

where $h_{i,\mathrm{ig}}$ is the ideal gas enthalpy at a given temperature and h_i is the actual enthalpy. Because the temperature ranges used in these studies are much lower than the boiling point of typical ligands, δ_2 is taken as the ambient condition value. However, the solubility parameter varies strongly with temperature and pressure for compressed solvents as is evident in eq 6. Increasing solvent density leads to an increase in the solvent solubility parameter and a corresponding decrease in the χ parameter. The observed reduced dispersibility of dodecanethiol-coated silver nanocrystals with decreased ethane density follows the lower critical solution temperature (LCST) phase behavior characteristic of low molecular weight solutes and polymers in SCFs. The solubility of a polymer in a supercritical fluid can be approximated with Hildebrand solubility parameters of the polymer segments and the solvent.[92] In SCFs, the cohesive energy density depends on the solvent density and an effective χ may be calculated to approximate solvent quality.[29,46]

Nanocrystal Dispersibility in Carbon Dioxide. The tails designed for low molecular weight surfactants in W/C microemulsions, e.g., fluoroakanes and fluorethers, provided insight useful for the design of thiol ligands for nanocrystal dispersions. Although short hydrocarbon molecules, such as decane readily dissolve in sc-CO_2, dodecanethiol-capped nanocrystals do not disperse in sc-CO_2 at conditions as high as 345 bar and 25 °C. In fact, we have only achieved dispersibility of dodecanethiol-coated silver nanocrystals with the addition of at least 50% (v/v) hexane as a cosolvent.[27] Hydrocarbon capping ligands are not solvated sufficiently by the weak van der Waals forces between CO_2 molecules to prevent flocculation between ligands. To achieve dispersibility in CO_2, we have developed "CO_2-philic" fluorinated stabilizing ligands.[27,33] Polymers made up of fluoroethers, fluoroacrylates, siloxanes, and branched hydrocarbons have proven to be soluble in sc-CO_2, as their weak van der Waals forces are consistent with those of CO_2.[41] The first example of nanocrystals dispersed in CO_2 with a capping ligand was achieved by using perfluorodecanethiol, a molecule similar to decanethiol, with the exception that the last eight carbons are fluorinated ($C_8F_{17}C_2H_4SH$). The fluorinated tail provides the solvent compatibility necessary to disperse the nanocrystals in CO_2.[27] In comparison, perfluorooctanethiol, which is only two fluorocarbons shorter, does not provide adequate steric repulsion to overcome the van der Waals attraction between the cores.[93] Recently, two more families of fluorinated surfactants have been found to disperse nanocrystals in CO_2 more effectively than the fluoroalkanes: perfluoropolyether (PFPE) and fluorooctyl methacrylate (FOMA)-based ligands. Perfluoropolyether-based thiols ($F(CF(CF_3)CF_2O)_3CF(CF_3)CONH(CH_2)_2SH$) dispersed nanocrystals in CO_2 at moderate pressures, allowing dispersibility of small gold nanocrystals, ~20 Å in diameter, in liquid CO_2 at the vapor pressure.[33] However, the most effective thiol to date is a fluorooctyl methacrylate-based thiol, ($CF_3(CF_2)_5CH_2CH_2OCOCH_2CH_2SH$) which could be used to disperse larger gold nanocrystals, 35 Å diameter, in liquid CO_2 at the vapor pressure.[33] Nanocrystal dispersibility in CO_2 follows qualitatively the same density dependence as in ethane, with increasing density leading to greater steric repulsion and increased dispersibility. In addition, larger particles exhibit greater interparticle interactions and require correspondingly higher solvent density to be dispersed.[28]

Fluorocarbon-coated nanocrystals exhibit dispersibility properties qualitatively different than alkanes, or hydrophilic ligands such as mercaptoacetic acid.[27] Fluorocarbon-capped nanocrystals disperse in fluorinated solvents such as Freon 113 (1,1,2 Trichlorotrifluoroethane) and Fluorinert (electronic liquid from 3M). Perfluoroalkanethiol-capped nanocrystals disperse in some polar solvents too, like acetone and ethanol, due to the significant dipole moment at the CH_2-CF_2 bond. However, none of these nanocrystals disperse in alkanes or typical nanocrystal solvents such as chloroform or toluene. The UV−visible absorbance spectra for silver nanocrystals capped with perfluorodecanethiol dispersed in sc-CO_2 showed a shift in plasmon peak position compared dispersions in acetone. The peak in the absorbance spectra corresponds to the lowest order surface mode, resulting from a plasma oscillation with uniform polarization across the volume of a nanocrystal. The resonant frequency of this oscillation, called the Fröhlich frequency ω_F, depends on particle size, the dielectric properties of the surrounding medium, and the plasmon energy for silver, ω_P. In the limit of small particle size, ω_F relates to the optical dielectric constant of the surrounding medium (which is the refractive index squared), by the following equation: $\omega_F^2 = \omega_P^2/\sqrt{1+2\epsilon_m}$. On the basis of the fact that $\epsilon_m(\text{acetone}) > \epsilon_m(CO_2)$, λ_{max} is expected to be lower for CO_2 compared to acetone. However, an observed increase in λ_{max} for nanocrystals dispersed in sc-CO_2 indicates an increase in particle size[27] that must be due to reversible particle "sticking" as a result of higher interparticle attractions in sc-CO_2 relative to acetone. Recently, small-angle X-ray scattering measurements have shown that even at sufficient densities to disperse nanocrystals, the particles may exist as small aggregated clusters due to the weak solvation of the ligand by CO_2.[94]

Finally, the edge-to-edge separation distance for fluorocarbon-coated nanocrystals is significantly larger than those capped with hydrocarbons.[27,33] For example, the edge-to-edge separation distance of nanocrystals deposited in a close packed layer on a substrate is ~22 Å for perfluorodecanethiol-capped nanocrystals compared to ~12.5 Å for decanethiol-capped nanocrystals. The stiffer fluorocarbon monolayer[95] maintains a greater particle separation distance.

Nanocrystal Monolayers Assembled from CO_2. Nanocrystals have been considered as "building blocks" that would potentially be assembled into superstructures with unique tunable properties. The physical properties of nanocrystal assemblies depend on both the nanocrystal size and electronic coupling between particles. Differences in the degree of ordering[96] and the particle separation distance[97] can lead to qualitative changes in the electronic properties of silver nanocrystal assemblies, as they can exhibit either insulating or metallic behavior depending on their superstructure. In addition, application into device structures requires consistency between samples, which is most readily achieved by using monodisperse nanocrystals organized into ordered lattice structures. Although Langmuir−Blodgett films have proven to be effective for relatively long-range ordering of nanocrystal monolayers, the technique is inefficient and impractical for industrial purposes. Drop-casting or spin-coating nanocrystals dispersed in volatile solvents allows fast organization of nanocrystals into ordered assemblies. However, instabilities in thin films of evaporating liquids, such as Marangoni convection and film dewetting seriously limit the extent of monolayer formation using conventional solvents.

The ability to disperse nanocrystals in liquid CO_2 at the vapor pressure opens up the possibility of using a compressed liquid solvent to deposit nanocrystal films. Relative to conventional

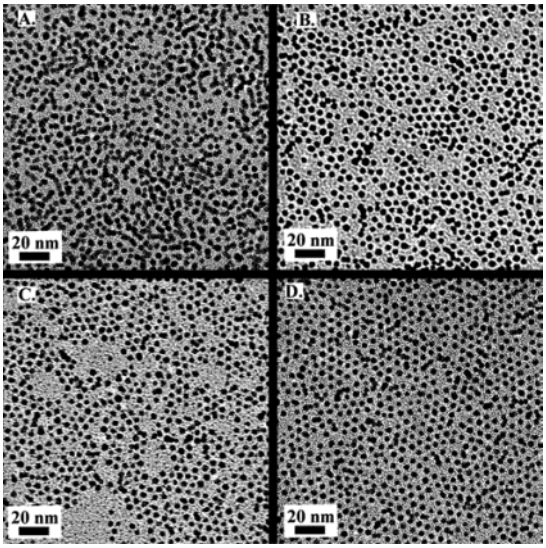

Figure 7. TEM images of perfluorooctyl methacrylate thiol-capped gold nanocrystals deposited from *l*-CO_2 at evaporation rates: (A) 1.027 μL/s; (B) 0.809 μL/s; (C) 0.388 μL/s; (D) 0.201 μL/s. Reproduced with permission from Shah et al. (*Nano Lett.* **2003**, *3*, 1671−1675). Copyright 2003 American Chemical Society.

solvents, a compressed solvent provides lower surface tension, controllable evaporation rates and a reduced tendency to dewet. The difference between conventional and compressed solvents is exemplified by examining the free energy required to form a dewetting hole in a thin liquid film.

$$\Delta G = 2\pi R\gamma t + \pi R^2\left(S - \frac{A_{132}}{t^2}\right) - \frac{\pi R^2 t}{\Omega}\Delta\mu \qquad (7)$$

Here R is the hole radius, t is the film thickness and Ω is the molecular volume. For volatile solvents, the chemical potential difference between the solvent and the vapor ($\Delta\mu$) that drives evaporation can cause a thin film of solvent to dewet even if the polar (S) and dispersion forces (A_{132}) favor wetting.[98−100] Dewetting leads to holes in the solvent film which can carry nanocrystals at the solvent/vapor interface as the hole expands during evaporation, leaving a nanocrystal monolayer laced with regions of exposed substrate. Comparatively, the chemical potential difference for a compressed solvent like liquid CO_2 is much lower, allowing as fast, or even faster, evaporation rates without destabilization of the thin solvent film.[33]

The first nanocrystal monolayers deposited from a compressed solvent consisted of FOMA-SH-capped gold nanocrystals (35 Å diameter) drop-cast from liquid CO_2 at the vapor pressure.[33] The experiments were performed in a high-pressure cell with tightly controlled evaporation rates. Figure 7 shows TEM images of nanocrystal monolayers drop-cast from CO_2 as a function of evaporation rate. The monolayers were prepared from the same batch of particles with identical size distributions. Fast evaporation leads to structurally disordered assemblies (Figure 7A) whereas slower evaporation rates deposit ordered structures (Figure 7D).

The translational correlation function, $g(r)$, and the orientational correlation function, $g_6(r)$, clearly revealed the increased structural order with decreased evaporation rate (Figure 8). The translational correlation function, $g(r)$, reflects the particle density $n(r)$, at distance r from a reference particle, normalized by the average particle density with increased peaks indicating longer range order. The orientational correlation function, $g_6(r)$, is determined from an order parameter $\psi_6^{(j)}$, which measures the orientation angle θ_{jk}, between a reference particle j, and its z nearest neighbors. The scaling of the orientational correlation function determines the crystal structure: liquids with $g_6(r) \sim \exp(-\xi r)$, a hexatic phase with $g_6(r) \sim r^{-\xi}$ and crystalline systems with $g_6(r) \sim$ constant, where ξ represents the inverse of the range of order. The faster than linear decay of experiments A−C, indicate liquidlike order in the monolayer even though the TEM images show short range order. Experiment D, however, displays a sharp contrast in structure, as $g_6(r)$ follows a linear decay indicating a hexatic phase.

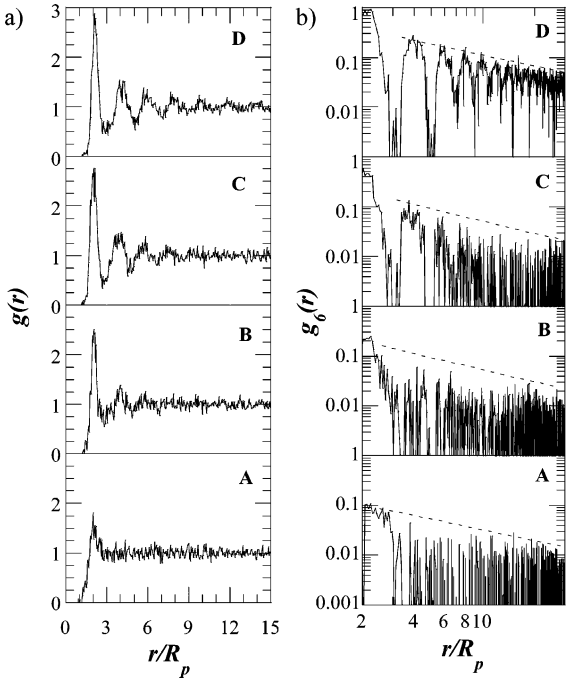

Figure 8. (a) Translational correlation function, $g(r)$, and (b) orientational correlation function, $g_6(r)$, for monolayers deposited from liquid CO_2 (shown in Figure 7). Reproduced with permission from Shah et al. (*Nano Lett.* **2003**, *3*, 1671−1675). Copyright 2003 American Chemical Society.

Converting the translational correlation function into a translational order parameter (T) and comparing to a reference state allow the degree of superlattice crystallization to be quantitatively examined as a function of evaporation rate. The translational order parameter is determined from the translational correlation function

$$T = \frac{\int_{R_p}^{R_c} |g(r) - 1| \mathrm{d}r}{R_c - R_p} \qquad (8)$$

with the integral evaluated from the particle radius R_p, to a cutoff distance R_c. The degree of crystallinity, φ, is then computed by comparing with the translational order parameter of the reference state T_{ref}: $\varphi = T/T_{ref}$. Shah et al. used a computer simulated random sequential adsorption of hard disks in two-dimensions as a reference state.[101]

An Avrami analysis, $\ln(1 - \varphi) = -k\tau^n$, where τ is the evaporation time, k is the kinetic factor, and n is the time exponent, is used to model the organization of the monolayer as a two-dimensional crystallization process. On the basis of this analysis, the kinetics of nanocrystal organization were found to be relatively sluggish, with $\ln(1 - \varphi) \propto \tau^{0.43}$. The exponent $n = 0.43$ is significantly less than the value characteristic of diffusion limited assembly in two dimensions ($n = 1$), indicating that monolayer formation is controlled by rearrangement of

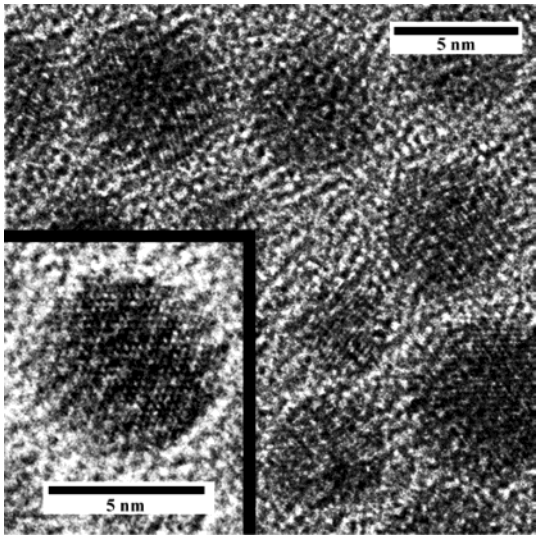

Figure 9. Representative TEM image of perfluorodecanethiol-capped silver nanocrystals synthesized in sc-CO_2. The inset shows high-resolution image with visible lattice fringes.

nanocrystal clusters rather than single particle diffusion. These studies also showed that evaporation rates of conventional volatile solvents must be slowed by at least an order of magnitude to achieve structures close to equilibrium.

Arrested Precipitation in CO_2. Most of the fluorocarbon-coated nanocrystals used to study dispersibility and deposition were synthesized in conventional solvents. Recently, silver, iridium, and platinum nanocrystals have been synthesized by arrested precipitation directly in pure sc-CO_2 by reducing CO_2-miscible organometallic precursors in the presence of capping ligands.[28,93] For example, silver nanocrystals were synthesized by reducing silver acetylacetonate with excess hydrogen in the presence of either perfluorodecanethiol or perfluorooctanethiol. The nanocrystals were collected and washed using acetone or Freon 113 and examined by TEM. Figure 9 shows TEM images of silver nanocrystals synthesized in CO_2. The visible lattice fringes indicate the crystalline quality of the cores.

The nanocrystal size distribution was found to be determined by the solvent density. Figure 10 shows the size and polydispersity of particles synthesized at various solvent pressures at constant temperature. By examining the size distribution moments (ratios of the mean radius, the cube mean radius, and harmonic mean radius), one can analyze the growth mechanism, and in particular the extent of coagulation versus condensation. At high solvent densities, with pressures exceeding 276 bar, the nanocrystals grow by a combination of coagulation and condensation. In this pressure range changes in the solvent density do not affect the average particle size and polydispersity. However, lowering the pressure below 276 bar, led to increased particle size and polydispersity. In this pressure range, particle growth occurs primarily by coagulation. At higher pressures, the ligand solvation is sufficient to provide adequate steric stabilization to prevent a large degree of coagulation, which yields nanocrystals with smaller size and polydispersity. Dispersibility tests at the reaction temperature of 80 °C revealed that the change in growth mechanism with pressure at 276 bar, occurs at the solvent density where steric stabilization is lost. The loss of steric repulsion causes a fundamental change in growth mechanism as partially capped cores are not as effectively protected from coagulation.[28]

Precursor concentration also affects nanocrystal size under conditions of poor steric stabilization. Under good solvent

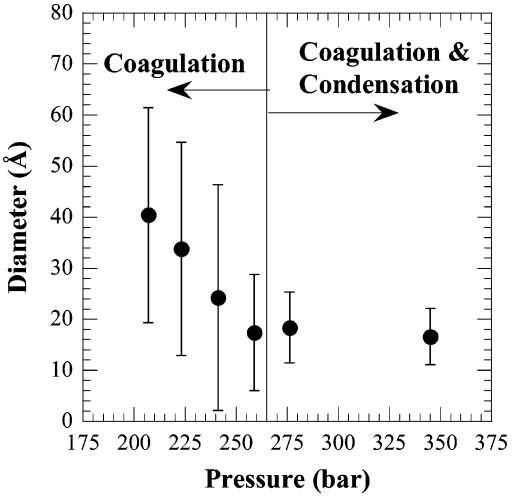

Figure 10. Average nanocrystal size of silver nanocrystals synthesized in sc-CO_2 at 80 °C as a function of pressure. The error bars represent the polydispersity of the sample. Coagulation and condensation growth was determined from the moments of the size distribution. Adapted with permission from Shah et al. (*J. Phys. Chem. B* **2002**, *106*, 12178−12185). Copyright 2002 American Chemical Society.

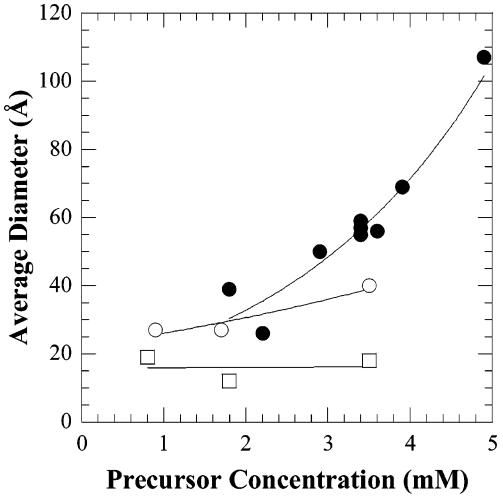

Figure 11. Average nanocrystal size of silver nanocrystals synthesized in sc-CO_2 as a function of precursor concentration: (□) 80 °C and 272 bar with perfluorodecanethiol capping ligands; (○) 80 °C and 207 bar with perfluorodecanethiol capping ligands; (●) perfluorooctanethiol-capped nanocrystals at various pressures and temperatures. Adapted with permission from Shah et al. (*J. Phys. Chem. B* **2001**, *105*, 9433−9440; **2002**, *106*, 12178−12185). Copyrights 2001 and 2002 American Chemical Society.

conditions with strong steric repulsion between particles, i.e., high solvent density with perfluorodecanethiol, the precursor concentration does not affect the particle size (Figure 11). At low solvent density, particle growth is dominated by coagulation and the particle size increases with higher precursor concentration. The shorter ligand, perfluorooctanethiol, provides only limited steric repulsion under all solvent conditions and the growth mechanism was dominated by coagulation at all solvent densities examined. In the coagulation dominated system, increasing precursor concentration leads to an increase in the number of initial nuclei and therefore higher collision rates between growing cores. However, despite the qualitative difference in growth mechanism, all synthetic conditions led to nanocrystals with complete ligand monolayer coverage that quenched growth and stabilized nanocrystals that could be

precipitated, redispersed, and reprecipitated without significant changes in particle size.

Arrested Precipitation of Si and Ge Nanocrystals in High-Temperature SCFs. The synthesis of silicon and germanium semiconductor nanocrystals requires significantly elevated temperatures to achieve core crystallinity. By pressurizing the solvent above its critical point, solution-phase temperatures far exceeding the boiling point of conventional solvents can be reached. For example, hexane can be utilized as a solvent for synthetic reactions at 400 °C by pressurizing to 300 bar. The SCF solvent therefore provides access to temperatures typically associated with vapor-phase processes, with the desired characteristics of high solubility and capping ligand steric stabilization necessary for high throughput synthesis and control over particle size distributions. For example, crystalline Si and Ge nanocrystals have successfully been formed in supercritical solvents through the thermolytic degradation of organosilane or organogermane precursors.[13,36,102,103] The synthesis scheme for these two materials is very similar. A solution consisting of the organogermane or organosilane precursor and the surface passivating agent (typically a long chain alcohol or a long chain alkene) is introduced to the high-pressure reaction cell containing the supercritical fluid. For example, octanol-passivated Si nanocrystals with diameters ranging from 15 to 40 Å can be obtained by thermolysis of diphenyl silane in supercritical hexane at 450 °C and 365 bar.[13] Figure 12A shows a high-resolution TEM image of an isolated 40 Å diameter Si nanocrystal. Similarly, Ge nanocrystals have been synthesized in supercritical hexane and octanol with diameters ranging between 14 and 700 Å at reaction conditions of 400 to 450 °C and 207 bar[36] (Figure 12B). The organic monolayer stabilized Ge and Si nanocrystals can be dispersed in a variety of organic solvents including hexane, toluene, and chloroform. The nanocrystals can be synthesized with dimensions smaller than the Bohr exciton radius (for example 4.3 nm for Si and 24.3 nm for Ge) and exhibit optical and electronic properties influenced by quantum confinement. Size-tunable absorbance and photoluminescence spectra, such as the room-temperature single Si nanocrystal photoluminescence spectra shown in Figure 13,[102] have been observed in Si and Ge nanocrystals synthesized by arrested precipitation in high-temperature supercritical solvents.[13,36] These Si nanocrystals have also exhibited size-dependent electrochemical charging and the first example of electrogenerated chemiluminescence for solution-dispersed semiconductor nanocrystals.[103] These observed material properties reflect that the nanocrystals produced in the high-temperature environment have crystalline cores that are chemically well-passivated. It has been difficult to achieve these chemical properties in group IV semiconductor nanocrystals using conventional solvents heated to lower synthesis temperatures and reflects the potential applicability of supercritical solvents for the synthesis of a host of nanocrystalline materials with strong covalent bonding.

Copper Nanocrystals in sc-H_2O. Unlike CO_2 and hydrocarbon solvents, the density-dependent solvation properties of supercritical water relate to large changes in the dielectric constant due to significantly decreased hydrogen bonding at high pressures. For water at ambient conditions $\epsilon \approx 80$, however, under supercritical conditions (374 °C and 225 bar) $\epsilon \approx 5$, making the solvation characteristics much more like that of a hydrocarbon solvent. Ion solubility, which is high at ambient conditions, decreases with increased density, whereas organic molecule solubility increases significantly.[104] This has led to considerable effort to use supercritical water to hydrolyze metal salts, which are soluble at ambient conditions to form metal oxide particulates.[105,106] Typically, the high temperatures aid in the crystallization of the material; however, agglomeration and coalescence must be avoided. By using organic capping ligands that are miscible with supercritical water to arrest the particle growth, coalescence can be prevented and particle size maintained.

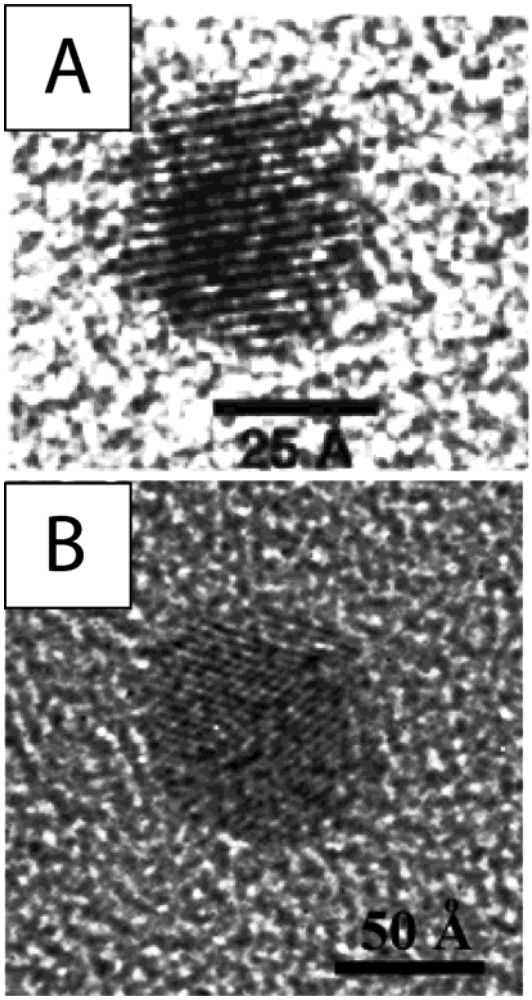

Figure 12. (a) High-resolution TEM image of a single 40 Å diameter Si nanocrystal showing the 3.1 Å (111) planes of the diamond lattice. Reproduced with permission from Holmes et al. (*J. Am. Chem. Soc.* **2001**, *123*, 3743−3748). Copyright 2001 American Chemical Society. (b) High-resolution TEM image of an isolated 57 Å diameter Ge nanocrystal.

Ziegler et al. recently employed alkanethiol as a capping ligand to control particle formation in supercritical water. Depending on the synthetic conditions, copper metal and copper oxide nanocrystals could be synthesized by hydrolyzing copper salts in supercritical water.[14] Cu nanocrystals with an average diameter of 70 Å were synthesized at 400 °C and 200 bar using copper nitrate as the precursor in the presence of hexanethiol. Increasing the temperature to 425 and 450 °C increased the average particle size to 78 and 92 Å, respectively. These nanocrystals were spherical, highly crystalline and protected from agglomeration by the thiol passivating layer. In the absence of the thiol, larger ($D_{av} \approx 160$ Å) CuO nanocrystals formed, which were agglomerated. Increasing the starting pH of the system from 3.4 to 6.0, through the addition of NaOH, led to much larger particles ($D_{av} = 400+$ Å) that were a mix of Cu and Cu_2O. This pH dependence appears to relate to the thermodynamic favoring of reactions with −OH groups that are

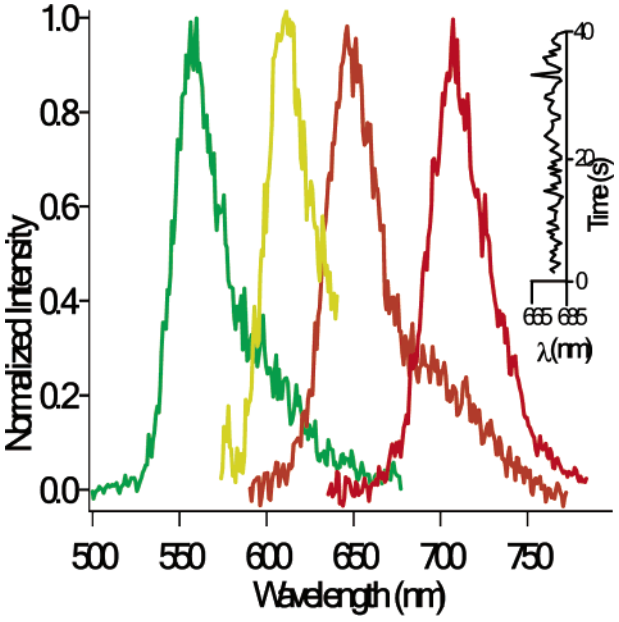

Figure 13. Four room-temperature PL spectra from individual Si nanocrystals measured by scanning confocal microscopy, showing narrow line widths and spectral tunability. Inset: mean spectral trajectory of a single particle showing that spectral diffusion is not observable within the experimental accuracy of the instrumentation. Reproduced with permission from English et al. (*Nano Lett.* **2002**, *2*, 681−685). Copyright 2002 American Chemical Society.

not as predominant at lower pH.[107] Ziegler et al. proposed a mechanism for sterically stabilized nanocrystal growth in supercritical water based on competing pathways of hydrolysis to large oxidized copper particles versus exchange of thiol ligands for anions to reduce copper cations to arrest growth by surface adsorption to stabilize Cu nanoparticles. The synthesis using copper acetate led to significantly larger nanocrystals (D_{av} = 340 Å) consisting of a mix of Cu and Cu_2O. Consistent with the proposed mechanism, it appears that the thiol could not effectively reduce copper ions when using the acetate precursor due to the stronger copper−anion complex formed with acetate compared to nitrate.

V. Supercritical Fluid−Liquid−Solid (SFLS) Nanowire Synthesis

Though there are many parallels between the synthesis of nanocrystals and nanowires in supercritical fluids, the processes involved in nucleation and growth of these nanostructures are quite different. Research in metal-seeded semiconductor nanowire growth originated from whisker growth studies in the 1960s, when Wagner and Ellis synthesized micrometer scale whiskers in a CVD reactor by decomposing Si precursor in the presence of Au seed droplets on a substrate.[108,109] The whisker growth process was described by the vapor−liquid−solid (VLS) mechanism (Figure 14) in which the semiconductor dissolves in the seed metal to form a liquid alloy that absorbs precursor material from the vapor until exceeding the saturation limit, when the semiconductor nucleates and grows in the form of a crystalline whisker. The minimum whisker diameter in the early studies was limited by the size of the smallest thermodynamically stable liquid Au seed droplet (~100 nm). The VLS approach was later applied toward the synthesis of nanometer size whiskers, or nanowires, by Lieber and co-workers who used laser ablation to generate nanometer scale metal seed particles to nucleate nanowire growth. This approach was extended toward the synthesis of a variety of semiconductor materials

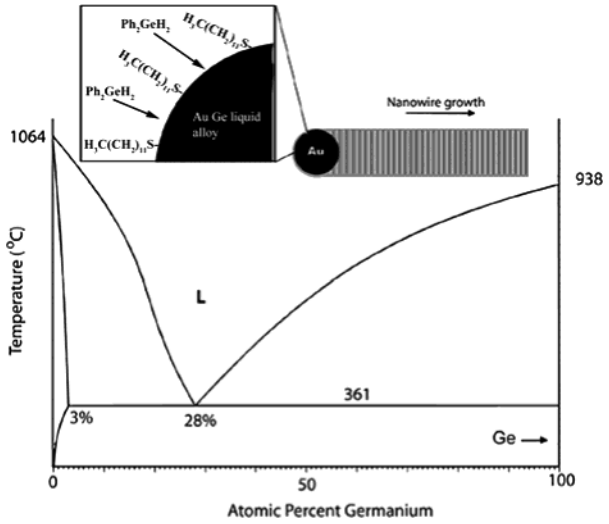

Figure 14. Binary phase diagram for the Au−Ge system with schematic illustration of nanowire growth. Reproduced with permission from Hanrath et al. (*Adv. Mater.* **2003**, *15*, 437−440). Copyright 2003 Wiley-VCH.

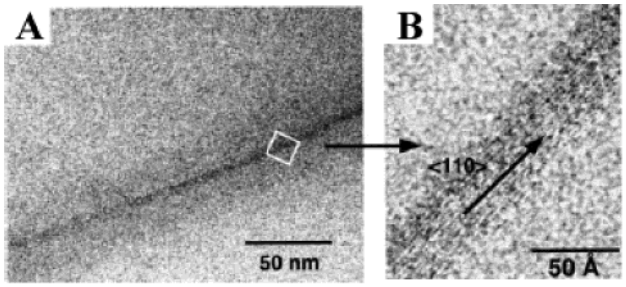

Figure 15. Low- (A) and high-resolution (B) TEM image of single-crystal Si nanowires synthesized at 500 °C in hexane at 270 bar. Visible are the (111) planes, separated by 3.14 Å orthogonal to the (110) growth axis. Nanowire samples were prepared for imaging by dispersing in chloroform and evaporating onto a carbon-coated copper TEM grid. Adapted with permission from Holmes et al. (*Science* **2000**, *287*, 1471−1473). Copyright 2000 AAAS.

including Si, Ge, and GaAs[110−112] but was limited by the broad size distribution of the laser ablation generated metal seed particles. A significant extension of the vapor-phase work was made by Buhro and co-workers who demonstrated VLS-type growth in solution for GaAs nanowires.

Silicon and Germanium Nanowires from Gold Nanocrystal Seeds. For better control of the optoelectronic properties of Si nanowires, it was desirable to form nanowires with specific and monodisperse diameters. In 2000, Holmes et al. first demonstrated that relatively monodisperse gold nanocrystals capped with dodecanethiol could effectively be used to seed the growth of Si nanowires smaller than 100 Å in diameter and micrometers in length, in supercritical hexane (Figure 15).[19] Whereas liquid solvents boil away at these temperatures, the supercritical hexane solvates the stabilizing ligands on the gold nanocrystals. Visible photoluminescence due to quantum confinement effects was observed as were discrete optical transitions in the UV−visible absorbance spectra. Lieber and co-workers later reported diameter control of Si and InP nanowires by combining CVD with size-monodisperse Au particles ranging in size from 5 to 30 nm attached to a surface.[113,114] In addition to providing nucleation seeds superior to those attained with the laser ablation approach, the supercritical fluid process has the added advantage of being scaleable to the synthesis of technologically significant quantities of nanowires.

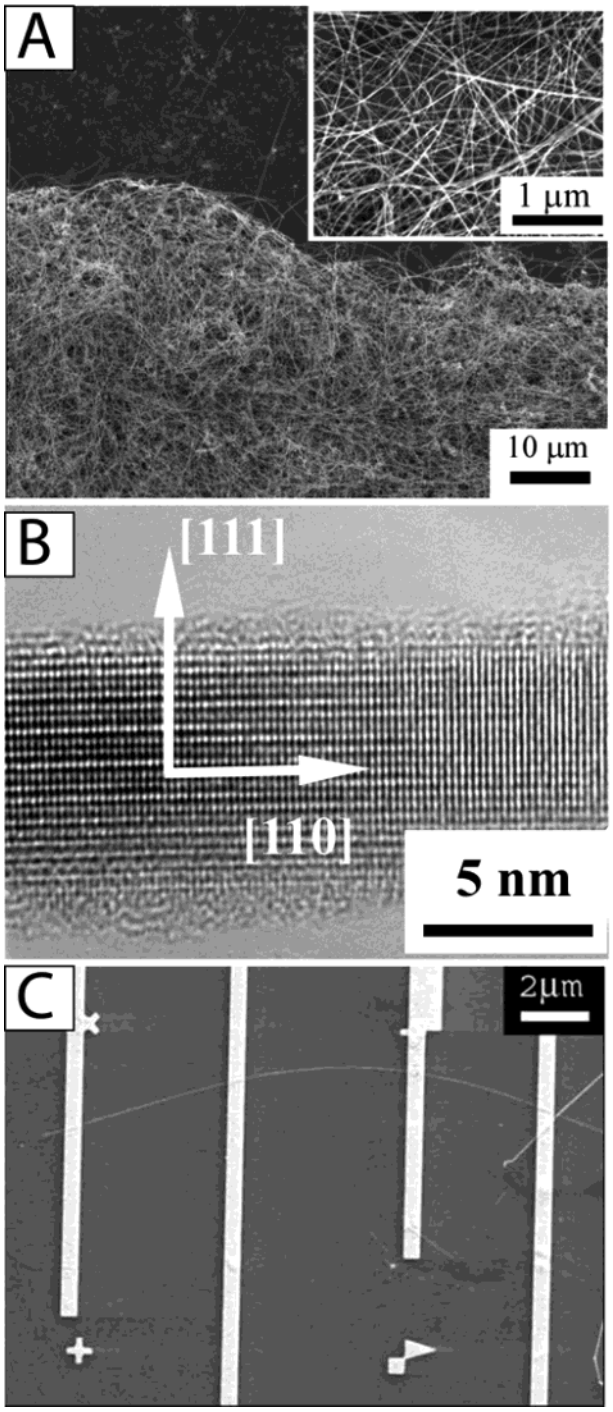

Figure 16. Images of Ge nanowires: (A) SEM of a carpet of Ge nanowires on a Si substrate as produced in the supercritical reactor (inset: higher magnification SEM image of the nanowire ensemble); (B) HRTEM image of a 75 Å diameter Ge nanowire with (110) crystallographic growth direction (the (220) planes are visible on the right side of the wire oriented perpendicular to the growth direction, and the (111) planes are visible on the left side of the wire extending parallel to the growth direction); (C) SEM image of a four terminal Ge nanowire device fabricated with Cr/Au contact electrodes.

We have extended the supercritical fluid approach to the synthesis of milligram quantities of high-quality single-crystal Ge nanowires with narrow diameter distributions.[37,38] The raw Ge nanowire product obtained with this technique consists of a dense mesh of long entangled nanowires, as shown in the HRSEM image in Figure 16A. HRTEM has shown that these Ge nanowires are single crystal with few crystalline defects and

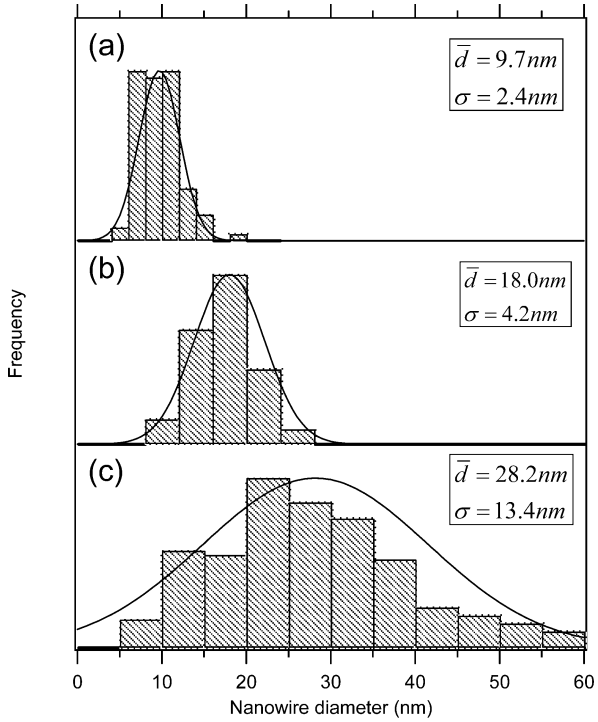

Figure 17. Histograms of the nanowire diameter size distributions produced by various modifications to the supercritical fluid synthesis. (a) Batch reaction with single injection followed up by pressurization (total injection time about 50−60 s). (b) Semibatch reaction with rapid injection of Au seed nanocrystals and 100 mM diphenylgermane precursor solution. (c) Continuous flow reaction with a reduced diphenylgermane concentration of 10 mM to limit seed droplet aggregation prior to nanowire nucleation.

a predominant [110] growth direction (see Figure 16B), although isolated occurrences of [111] growth have been observed. This material can be processed and redispersed to fabricate single nanowire electrical devices to study electron transport through the nanowires. Figure 16C shows a single nanowire device contacted by two metal source-drain electrodes which can be gated by applying a voltage from the back substrate. More recently, the supercritical fluid technique has been extended to the synthesis of group III−V compound semiconductor nanowires such as GaAs and GaP.[115]

To control the nanowire diameter distribution, nanocrystal agglomeration must be controlled in the reactor. The initial supercritical fluid nanowire synthesis in our laboratories used a batch reactor system, where the precursor material and the Au seed nanocrystals were injected into the reactor cell, similarly to the supercritical nanocrystal synthesis discussed above. To increase the yield, higher reactant concentrations are required, and the likelihood of aggregates increases. Under these conditions, the average nanowire diameter and the size distribution of the nanowires obtained using a batch approach are much larger than the diameter and distributions of the seed nanocrystals. This size broadening results from agglomeration of liquid seed droplets prior to nucleation and growth of the single crystal nanowire. In an effort to reduce size broadening of the seed droplet during these initial growth stages the reactor system was modified to quickly inject the solution containing precursor and Au seed nanocrystal into a preheated and pre-pressurized reactor. The histograms in Figure 17a,b show significant reduction in the average nanowire diameter and polydispersity accomplished through this modification.[116]

Additional improvements toward the synthesis of technologically significant quantities of high-quality, size monodisperse

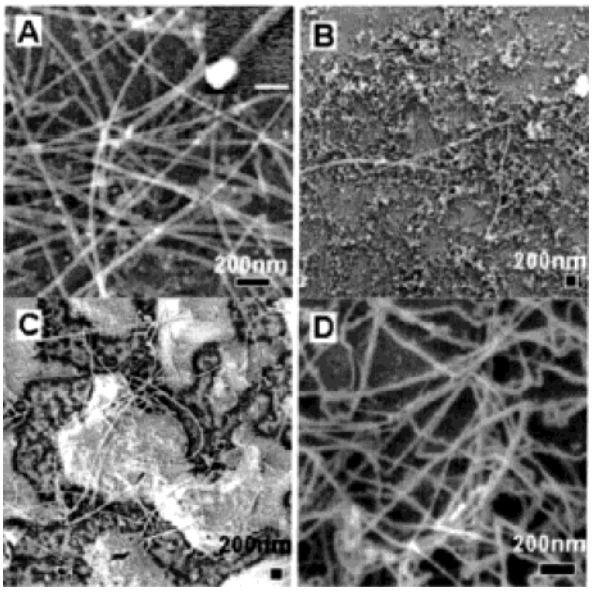

Figure 18. High-resolution SEM images of Si nanowires grown from Au nanocrystals tethered to a Si substrate. The nanowires were formed in a flow reactor from 250 mM solution of diphenylsilane at (a) 0.5 mL/min, 500 °C, (b) 1.0 mL/min, 500 °C, (c) 3.0 mL/min, 500 °C and (d) 0.5 mL/min, 450 °C. Reproduced with permission from Lu et al. (*Nano Lett.* **2003**, *3*, 93−99). Copyright 2003 American Chemical Society.

nanowires have been accomplished by converting the supercritical fluid method from an injection-based system to a continuous flow reactor. Compared to the batch and semicontinuous processes, the flow-through reaction is carried out with much lower precursor concentrations, which minimizes the agglomeration of the Au seeds during initial nucleation stages and, hence, reduces the average nanowire diameter and polydispersity.[116] This technique allows the production of high-quality Ge nanowires with a yield of approximately 80% at a rate of 10 mg/h. More importantly, the continuous nature of this approach permits scale-up for the synthesis of technologically significant quantities which cannot be met by CVD-based methods.

Seeded Nanowire Growth from Silicon Substrates. In an alternative approach aimed at the reduction of seed particle agglomeration, monodisperse Au nanocrystals were molecularly tethered to a silicon substrate as seeds for Si nanowire growth.[117] Rather than using free floating seed particles as in the synthesis schemes discussed above, this method is based on the covalent linkage of the seed particle to the substrate. This approach has two distinct advantages to the homogeneous process: first, undesired byproducts are easily removed from the synthesized nanowires during the synthesis and second, the continuous flow approach permits the precursor concentration in the reactor be maintained at a controlled value, thereby enabling the study of the critical kinetic growth factors involved in nanowire nucleation and growth. The supply rate of Si to the seed particle can be easily adjusted by changing the flow rate or concentration of the precursor solution or by adjusting the decomposition kinetics through changes in the synthesis temperatures.

Figure 18 illustrates how these factors influence the morphology of the nanowires grown from the tethered seed particles.[112] At low Si supply rates, curly nanowires with many crystallographic defects are obtained, indicating starvation of growth sites (see Figure 18D). An excess supply of Si will overwhelm the tethered Au nucleation sites and lead to the formation of Si particles through homogeneous nucleation (Figure 18B,C). Under optimized conditions, this approach allows the synthesis of significant quantities of high-quality Si nanowires (Figure 18A). In addition to the synthesis advantages discussed above, this approach also demonstrates an important first step toward the integration of nanowire synthesis and ordered assembly which is desirable for future technological applications of nanowires.

Nanowire Growth in Templated Structures. Early attempts to use mesoporous solids as templates for the gas-phase growth of semiconductor materials have met limited success.[118] Recently, however, Holmes and co-workers utilized the unique characteristics of supercritical fluids, particularly high diffusivities, in combination with mesoporous templates to direct the formation of high-density three-dimensional arrays of semiconductor nanowires.[39,119,120] In their approach, the degraded precursor material is not directed toward one-dimensional crystallization by the presence of a seed crystal, instead, the one-dimensional structures are obtained as the material fills the nanometer wide channels of the silica matrix. This technique presents a facile way to produce significant quantities of nanowires while at the same time ordering them in hierarchical structures. The confinement of the semiconductor nanowires within the pores of this silica matrix has shown that the optical properties of the nanowires can be tuned over a wide energy range by choosing host matrixes with different pore dimensions. In a recent modification to the supercritical fluid inclusion phase technique, Ryan et al.[121] have used mesoporous thin films on silicon and quartz substrates to synthesize ultrahigh-density arrays of aligned Ge nanowires from supercritical CO_2, oriented almost perpendicular to the substrate. Their work illustrates that supercritical fluids not only provide excellent physicochemical properties for the controlled synthesis of nanowires but also provide an environment for the hierarchical "bottom up" assembly of nanostructures.

VI. Concluding Remarks and Future Directions

SCFs offer unique solvent properties useful for nanocrystal and nanowire synthesis and chemical processing. The flexibility of SCFs, in terms of tunable solvation strength and access to high operating temperatures and pressures, enables the synthesis of a variety of nanostructured metal and semiconductor materials. The enhanced wettability and controlled solvation strength provide a medium in which the fundamentals of nanocrystal growth and assembly can be studied in a manner not previously possible. Examples include the effect of steric repulsion on nanocrystal growth and an elucidation of nanocrystal organization kinetics in the formation of 2D lattices. These fundamental studies have been carried over to nanowire synthesis where wire morphology has been studied as a function of reaction conditions.

In addition to fundamental studies, SCFs provide unique processing advantages over conventional solvents and gas phase approaches. Using SCFs for nanocrystal separation allows reversible size-dependent dispersibility with slight changes in temperature and pressure. Particle size, polydispersity, and growth mechanism during nanocrystal synthesis can be controlled explicitly through the variation of carbon dioxide density. Ordered nanocrystal lattices can be cast faster using liquid carbon dioxide than conventional solvents because of a smaller tendency for solvent dewetting. Additionally, the high operating temperatures achievable in supercritical fluids enables the crystallization of important semiconductor nanocrystal materials such as Si and Ge. The increased solvation power of SCFs compared to gases allows increased precursor concentrations,

enabling the synthesis of technologically significant quantities of nanocrystals and nanowires. Finally, SCFs allow the synthesis of densely packed nanowires in ordered templates by eliminating solvent wetting limitations.

Currently, efforts continue to gain a better understanding of the possibilities as well as the limitations in using SCFs for nanomaterial processing. High-pressure experimental techniques are being devised to measure the interactions between nanocrystals dispersed in compressible solvents. In addition, simulations to understand the effect of ligand architecture on steric repulsion are also underway. By comparing experimental and simulated results, one can develop different ligand architectures that can be tailored to specific applications and still allow SCF dispersibility. Studies to elucidate the exact physical processes involved in the luminescence of Si nanostructures are also ongoing. In addition, optimization of the reaction conditions to increase yield while minimizing reaction byproducts are being examined. However, even with the current synthetic limitations in these systems, several applications such as Si nanocrystals light emitting devices have already been proposed. Untreated surfaces of Ge nanowires oxidize, rendering the wires chemically unstable and electrically defective. To address this issue, developments are underway for in situ chemical surface modifications to passivate the nanowire surface. Further chemical functionalization for sensor devices are currently being studied as well.

Acknowledgment. This work is supported in part by the STC Program of the National Science Foundation under Agreement No. CHE-9876674, the Welch Foundation (K.P.J. and B.A.K.), the Department of Energy, and the ATP and ARP programs of the Texas Higher Educating Coordinating Board. We thank Xianmao Lu for the Ge TEM and useful discussions. We also thank Christopher Kitchens and Christopher Roberts for Cu TEMs.

References and Notes

(1) Brus, L. *J. Phys. Chem.* **1986**, *90*, 2555.
(2) Chen, S.; Ingrma, R. S.; Hostetler, M. J.; Pietron, J. J.; Murray, R. W.; Schaaff, T. G.; Khoury, J. T.; Alvarez, M. M.; Whetten, R. L. *Science* **1998**, *280*, 2098.
(3) Murray, C. B.; Norris, D. J.; Bawendi, M. G. *J. Am. Chem. Soc.* **1993**, *115*, 8706−8715.
(4) Klein, D. L.; Roth, R.; Lim, A.; Alivisatos, A. P.; McEuen, P. L. *Nature* **1997**, *389*, 699.
(5) Empedocles, S. A.; Neuhauser, R.; Shimizu, K.; Bawendi, M. G. *Adv. Mater.* **1999**, *11*, 1243.
(6) Colvin, V. L.; Schlamp, M. C.; Alivisatos, A. P. *Nature* **1994**, *370*, 354.
(7) Alivisatos, A. P. *Science* **1996**, *271*, 933−937.
(8) Andres, R. P.; Bein, T.; Dorogi, M.; Feng, S.; Henderson, J. I.; Kubiak, C. P.; Mahoney, W.; Osifchin, R. G.; Reifenberger, R. *Science* **1996**, *272*, 1323−1325.
(9) Duan, X.; Huang, Y.; Cui, Y.; Wang, J.; Lieber, C. M. *Nature* **2001**, *409*, 66−69.
(10) Korgel, B. A.; Monbouquette, H. G. *J. Phys. Chem.* **1996**, *100*, 346−351.
(11) Guzelian, A. A.; Banin, U.; Kadavanich, A. V.; Peng, X.; Alivisatos, A. P. *Appl. Phys. Lett.* **1996**, *69*, 1432−1434.
(12) Brust, M.; Walker, M.; Bethell, D.; Schiffrin, D. J.; Whyman, R. *J. Chem. Soc., Chem. Commun.* **1994**, *7*, 801−802.
(13) Holmes, J. D.; Ziegler, K. J.; Doty, R. C.; Pell, L. E.; Johnston, K. P.; Korgel, B. A. *J. Am. Chem. Soc.* **2001**, *123*, 3743.
(14) Ziegler, K. J.; Doty, R. C.; Johnston, K. P.; Korgel, B. A. *J. Am. Chem. Soc.* **2001**, *123*, 7797−7803.
(15) Peng, X.; Manna, L.; Yang, W.; Wickham, J.; Scher, E.; Kadavanich, A.; Alivisatos, A. P. *Nature* **2000**, *404*, 59−61.
(16) Puntes, V. F.; Krishnan, K. M.; Alivisatos, A. P. *Science* **2001**, *291*, 2115−2117.
(17) Kan, S.; Mokari, T.; Rothenberg, E.; Banin, U. *Nature Mater.* **2003**, *2*, 155−158.
(18) Yu, H.; Buhro, W. E. *Adv. Mater.* **2003**, *15*, 416−419.
(19) Holmes, J. D.; Johnston, K. P.; Doty, R. C.; Korgel, B. A. *Science* **2000**, *287*, 1471.
(20) Eckert, C. A.; Knutson, B. L.; Debenedetti, P. G. *Nature* **1996**, *383*, 313−318.
(21) Harrison, K.; Goveas, J.; Johnston, K. P.; O'Rear, E. A. *Langmuir* **1994**, *10*, 3536−3541.
(22) Eastoe, J.; Bayazit, Z.; Martel, S.; Steytler, D. C.; Heenan, R. K. *Langmuir* **1996**, *12*, 1423−1424.
(23) Johnston, K. P.; Harrison, K. L.; Clarke, M. J.; Howdle, S. M.; Heitz, M. P.; Bright, F. V.; Carlier, C.; Randolph, T. W. *Science* **1996**, *271*, 624.
(24) Zielinski, R. G.; Kline, S. R.; Kaler, E. W.; Rosov, N. *Langmuir* **1997**, *13*, 3934−3937.
(25) Ji, M.; Chen, X.; Wai, C. M.; Fulton, J. L. *J. Am. Chem. Soc.* **1999**, *121*, 2631−2632.
(26) Holmes, J. D.; Bhargava, P. A.; Korgel, B. A.; Johnston, K. P. *Langmuir* **1999**, *15*, 6613−6615.
(27) Shah, P. S.; Holmes, J. D.; Doty, R. C.; Johnston, K. P.; Korgel, B. A. *J. Am. Chem. Soc.* **2000**, *122*, 4245−4246.
(28) Shah, P. S.; Husain, S.; Johnston, K. P.; Korgel, B. A. *J. Phys. Chem. B* **2002**, *106*, 12178−12185.
(29) Shah, P. S.; Holmes, J. D.; Johnston, K. P.; Korgel, B. A. *J. Phys. Chem. B* **2002**, *106*, 2545−2551.
(30) Brennecke, J. F.; Chateauneuf, J. E. *Chem. Rev.* **1999**, *99*, 433.
(31) Meredith, J. C.; Johnston, K. P. In *Supercritical Fluids Fundamentals and Applications*; Kiran, E., Peters, C., Eds.; Kluwer Academic Publishers: Dordrecht, The Netherlands, 2000; pp 211−228.
(32) Johnston, K. P.; DaRocha, S. R. P.; Holmes, J. D.; Jacobson, G. B.; Lee, C. T.; Yates, M. Z. In *Green Chemistry Using Liquid and Supercritical Carbon Dioxide*; DeSimone, J., Tumas, W., Eds.; Oxford University Press: Oxford, 2003; pp 134−148.
(33) Shah, P. S.; Novick, B. J.; Hwang, H. S.; Lim, K. T.; Carbonell, R. G.; Johnston, K. P.; Korgel, B. A. *Nano Lett.* **2003**, *3*, 1671−1675.
(34) Fukushima, Y.; Wakayama, H. *J. Chem. Phys. B* **1999**, *103*, 3062−3064.
(35) Blackburn, J. M.; Long, D. P.; Cabañas, A.; Watkins, J. J. *Science* **2001**, *294*, 141−145.
(36) Lu, X.; Ziegler, K. J.; Ghezelbash, A.; Johnston, K. P.; Korgel, B. A. *Nano Lett.* **2004**, *4*, 969−974.
(37) Hanrath, T.; Korgel, B. A. *J. Am. Chem. Soc.* **2002**, *124*, 1424.
(38) Hanrath, T.; Korgel, B. A. *Adv. Mater.* **2003**, *15*, 437.
(39) Holmes, J. D.; Lyons, D. M.; Ziegler, K. J. *Chem. Eur. J.* **2003**, *9*, 2144−2150.
(40) Sanchez, I. C.; Stone, M. T. In *Polymer Blends Volume 1: Formulation*; Bucknall, C. B., Ed.; John Wiley and Sons: New York, 2000.
(41) O'Neill, M. L.; Cao, Q.; Fang, M.; Johnston, K. P.; Wilkinson, S. P.; Smith, C. D.; Kerschner, J. L.; Jureller, S. H. *Ind. Eng. Chem. Res.* **1998**, *37*, 3067−3079.
(42) Peck, D. G.; Johnston, K. P. *Macromolecules* **1993**, *26*, 1537.
(43) Meredith, J. C.; Johnston, K. P. *Macromolecules* **1998**, *31*, 5518−5528.
(44) Meredith, J. C.; Sanchez, I. C.; Johnston, K. P.; Pablo, J. J. d. *J. Chem. Phys.* **1998**, *109*, 6424−6434.
(45) Yates, M. Z.; O'Neill, M. L.; Johnston, K. P.; Webber, S.; Canelas, D. A.; Betts, D. E.; DeSimone, J. M. *Macromolecules* **1997**, *30*, 5060−5067.
(46) Dickson, J. L.; Ortiz-Estradan, C.; Alvarado, J. F. J.; Hwang, H. S.; Sanchez, I. C.; Luna-Barcenas, G.; Lim, K. T.; Johnston, K. P. *J. Colloid Interface Sci. Technol.* **2004**, *272*, 444−456.
(47) Sirard, S. M.; Castellanos, H.; Hwang, H. S.; Lim, K. T.; Johnston, K. P. *Ind. Eng. Chem. Res.* **2004**, *43*, 525−534.
(48) Yates, M. Z.; Shah, P. S.; Johnston, K. P.; Lim, K. T.; Webber, S. *J. Colloid Interface Sci.* **2000**, *227*, 176−184.
(49) Sirard, S. M.; Gupta, R. R.; Russell, T. P.; Watkins, J. J.; Green, P. F.; Johnston, K. P. *Macromolecules* **2003**, *36*, 3365−3373.
(50) Hoefling, T. A.; Beitle, R. R.; Enick, R. M.; Beckman, E. J. *Fluid Phase Equilib.* **1993**, *83*, 203−212.
(51) McClain, J. B.; Londono, D.; Combes, J. R.; Romack, T. J.; Canelas, D. A.; Betts, D. E.; Wignal, G. D.; Samulski, E. T.; DeSimone, J. M. *J. Am. Chem. Soc.* **1996**, *118*, 917−918.
(52) O'Shea, K.; Kirmse, K.; Fox, M. A.; Johnston, K. P. *J. Phys. Chem.* **1991**, *95*, 7863.
(53) DeSimone, J. M.; Maury, E. E.; Menceloglu, Y. Z.; McClain, J. B.; Romack, T. J.; Combes, J. R. *Science* **1994**, *265*, 356.
(54) Lepilleur, C.; Beckman, E. J. *Macromolecules* **1997**, *30*, 745−756.
(55) Dickson, J. L.; Psathas, P. A.; Salinas, B.; Ortiz-Estrada, C.; Luna-Barcenas, G.; Hwang, H. S.; Lim, K. T.; Johnston, K. P. *Langmuir* **2003**, *19*, 4895.
(56) Eastoe, J.; Paul, A.; Nave, S.; Steytler, D. C.; Robinson, B. H.; Rumsey, E.; Thorpe, M.; Heenan, R. K. *J. Am. Chem. Soc.* **2001**, *123*, 988−989.
(57) Ryoo, W.; Webber, S. E.; Johnston, K. P. *Ind. Eng. Chem. Res.* **2003**, *42*, 6348.

(58) Lee, C. T.; Johnston, K. P.; Dai, H. J.; Cochran, H. D.; Melnichenko, Y. B.; Wignall, G. D. *J. Phys. Chem. B.* **2001**, *105*, 3540−3548.
(59) Stone, M. T.; Smith, P. G.; Rocha, S. R. P. d.; Rossky, P. J.; Johnston, K. P. *J. Phys. Chem. B* **2004**, *108*, 1962−1966.
(60) Watkins, J. J.; McCarthy, T. J. *Chem. Mater.* **1995**, *7*, 1991−1994.
(61) Brown, G. D.; Smith, S. D.; Watkins, J. J. *Polym. Mater. Sci. Eng.* **2000**, *82*, 292−293.
(62) Brown, G. D. In *Materials Issues and Modeling for Device Nanofabrication*; Whitman, L. J., Ed.; Materials Research Society Proceedings; MRS: Warrendale, PA, 2000; Vol. 584.
(63) Blackburn, J. M.; Long, D. P.; Watkins, J. J. *Chem. Mater.* **2000**, *12*, 2625−2631.
(64) Bartscherer, K. A.; Renon, H.; Minier, M. *Fluid Phase Equilib.* **1995**, *107*, 93−150.
(65) McFann, G. J.; Johnston, K. P. In *Microemulsions: Fundamental and Applied Aspects*; Kumar, P., Ed.; Dekker: New York, 1999; pp 281−307.
(66) Johnston, K. P.; Jacobson, G. B.; Lee, C. T.; Meredith, C.; DaRocha, S. R. P.; Yates, M. Z.; DeGrazia, J.; Randolph, T. W. In *Chemical Synthesis Using Supercritical Fluids*; Leitner, W., Ed.; Wiley-VCH: Weinheim, 1999; pp 127−146.
(67) Peck, D. G.; Johnston, K. P. *J. Phys. Chem.* **1993**, *97*, 5661.
(68) Ohde, H.; Hunt, F.; Wai, C. M. *Chem. Mater.* **2001**, *13*, 4130−4135.
(69) McLeod, M. C.; McHenry, R. S.; Beckman, E. J.; Roberts, C. B. *J. Phys. Chem. B* **2003**, *107*, 2693−2700.
(70) Ohde, H.; Ye, X.-R.; Wai, C. M.; Rodriguez, J. M. *Chem. Commun.* **2000**, 2353−2354.
(71) Ohde, H.; Ohde, M.; Bailey, F.; Kim, H.; Wai, C. M. *Nano Lett.* **2002**, *2*, 721−724.
(72) Cason, J. P.; Roberts, C. B. *J. Phys. Chem. B* **2000**, *104*, 1217−1221.
(73) Cason, J. P.; Miller, M. E.; Thompson, J. B.; Roberts, C. B. *J. Phys. Chem. B* **2001**, *105*, 2297−2302.
(74) Cason, J. P.; Khambaswadkar, K.; Roberts, C. B. *Ind. Eng. Chem. Res.* **2000**, *39*, 4749−4755.
(75) Kitchens, C. L.; McLeod, M. C.; Roberts, C. B. *6th International Symposium on Supercritical Fluids*; Versailles, France, April 2003; International Society for the Advancement of Supercritical Fluids: Nancy, France.
(76) Kitchens, C.; Roberts, C. B. *Ind. Eng. Chem. Res.* **2004**.
(77) Sun, Y.-P.; Rollins, H. W.; Guduru, R. *Chem. Mater.* **1999**, *11*, 7−9.
(78) Sun, Y.-P.; Guduru, R.; Lin, F.; Whiteside, T. *Ind. Eng. Chem. Res.* **2000**, *39*, 4663−4669.
(79) Sun, Y.-P.; Rollins, H. W. *Chem. Phys. Lett.* **1998**, *288*, 585−588.
(80) Sun, Y.-P.; Atorngitjawat, P.; Meziani, M. J. *Langmuir* **2001**, *17*, 5707−5710.
(81) Dixon, D. J.; Bodmeier, R. A.; Johnston, K. P. *AIChE J.* **1993**, *39*, 127.
(82) Randolph, T. W.; Randolph, A. D.; Mebes, M.; Yeung, S. *Biotechnol. Prog.* **1993**, *9*, 429−435.
(83) Yeo, S. D.; Debenedetti, P. G.; Radosz, M.; Schmidt, H. W. *Macromolecules* **1993**, *26*, 6207−6210.
(84) Reverchon, E. *J. Supercrit. Fluids* **1999**, *15*, 1−21.
(85) Chattopadhyay, P.; Gupta, R. B. *Ind. Eng. Chem. Res.* **2000**, *39*, 2281−2289.
(86) Hamaker, H. C. *Physica* **1937**, *4*, 1058−1072.
(87) Israelachvili, J. *Intermolecular & Surface Forces*; 2nd ed.; Academic Press: San Diego, 1992.
(88) Lewis, J. E.; Biswas, R.; Robinson, A. G.; Maroncelli, M. *J. Phys. Chem. B* **2001**, *105*, 3306−3318.
(89) Romero-Cano, M. S.; Puertas, A. M.; de la Nieves, F. J. *J. Chem. Phys.* **2000**, *112*, 8654−8659.
(90) Vincent, B.; Edwards, J.; Emmett, S.; Jones, A. *Colloids Surf.* **1986**, *18*, 261−281.
(91) Clarke, N. Z.; Waters, C.; Johnson, K. A.; Satherley, J.; Schiffrin, D. J. *Langmuir* **2001**, *17*, 6048−6050.
(92) Shine, A. D. In *Physical Properties of Polymers Handbook*; Mark, J. E., Ed.; AIP: Cincinnati, OH, 1996; pp 249−256.
(93) Shah, P. S.; Husain, S.; Johnston, K. P.; Korgel, B. A. *J. Phys. Chem. B* **2001**, *105*, 9433−9440.
(94) Saunders, A. E.; Shah, P. S.; Park, E. J.; Lim, K. T.; Johnston, K. P.; Korgel, B. A. *J. Phys. Chem. B*, submitted for publication.
(95) Chidsey, C. E. D.; Loiacono, D. N. *Langmuir* **1990**, *6*, 682−691.
(96) Doty, R. C.; Yu, H.; Shih, C. K.; Korgel, B. A. *J. Phys. Chem. B* **2001**, *105*, 8291−8296.
(97) Collier, C. P.; Saykally, R. J.; Shiang, J. J.; Henrichs, S. E.; Heath, J. R. *Science* **1997**, *277*, 1978−1981.
(98) Schenning, A. P. H. J.; Benneker, F. B. G.; Geurts, H. P. M.; Liu, X. Y.; Nolte, R. J. M. *J. Am. Chem. Soc.* **1996**, *118*, 8549−8552.
(99) Ohara, P. C.; Gelbart, W. M. *Langmuir* **1998**, *14*, 3418−3424.
(100) Elbaum, M.; Lipson, S. G. *Phys. Rev. Lett.* **1994**, *72*, 3562−3565.
(101) Gray, J. J.; Klein, D. H.; Korgel, B. A.; Bonnecaze, R. T. *Langmuir* **2001**, *17*, 2317−2328.
(102) English, D. S.; Pell, L. E.; Yu, Z.; Barbara, P. F.; Korgel, B. A. *Nano Lett.* **2002**, *2*, 681.
(103) Ding, Z.; Quinn, B. M.; Haram, S. K.; Pell, L. E.; Korgel, B. A.; Bard, A. J. *Science* **2002**, *296*, 1293−1297.
(104) Savage, P. E.; Gopalan, S.; Mizan, T. I.; Martino, C. J.; Brock, E. E. *AIChE J.* **1995**, *41*, 1723.
(105) Adschiri, T.; Kanazawa, K.; Arai, K. *J. Am. Ceram. Soc.* **1992**, *75*, 2615−2618.
(106) Adschiri, T.; Hakuta, Y.; Arai, K. *Ind. Eng. Chem. Res.* **2000**, *29*, 4901−4907.
(107) Beverskog, B.; Puigdomenech, I. *J. Electrochem. Soc.* **1997**, *144*, 3476−3483.
(108) Wagner, R. S.; Ellis, W. C. *Appl. Phys. Lett.* **1964**, *4*, 89.
(109) Wagner, R. S.; Ellis, W. C.; Jackson, K. A.; Arnold, S. M. *J. Appl. Phys.* **1964**, *35*, 2993.
(110) Morales, A. M.; Lieber, C. M. *Science* **1998**, *279*, 208.
(111) Duan, X.; Lieber, C. M. *J. Am. Chem. Soc.* **2000**, *122*, 188.
(112) Hu, J.; Odom, T. W.; Lieber, C. M. *Acc. Chem. Res.* **1999**, *32*, 435.
(113) Gudiksen, M. S.; Wang, J.; Lieber, C. M. *J. Phys. Chem. B* **2001**, *105*, 4062.
(114) Cui, Y.; Lauhon, J.; Gudiksen, M. S.; Wang, J.; Lieber, C. M. *Appl. Phys. Lett.* **2001**, *78*, 2214.
(115) Davidson, F. M., III; Schricker, A. D.; Wiacek, R. J.; Korgel, B. A. *Adv. Mater.* **2004**, *16*, 646−649.
(116) Hanrath, T.; Lu, X.; Johnston, K. P.; Korgel, B. A. *Provisional Appl. 60/485,244* (USA).
(117) Lu, X.; Hanrath, T.; Johnston, K. P.; Korgel, B. A. *Nano Lett.* **2003**, *3*, 93.
(118) Moller, K.; Bein, T. *Chem. Mater.* **1998**, *10*, 2950.
(119) Coleman, N. R. B.; O'Sullivan, N.; Ryan, K. M.; Crowley, T. A.; Morris, M. A.; Spalding, T. R.; Steytler, D. C.; Holmes, J. D. *J. Am. Chem. Soc.* **2001**, *123*, 7010.
(120) Coleman, N. R. B.; Ryan, K. M.; Spalding, T. R.; Holmes, J. D.; Morris, M. A. *Chem. Phys. Lett.* **2001**, *343*, 1.
(121) Ryan, K. M.; Erts, D.; Olin, H.; Morris, M. S.; Holmes, J. D. *J. Am. Chem. Soc.* **2003**, *125*, 6284.
(122) Fulton, J. L.; Smith, R. D. *J. Phys. Chem.* **1988**, *92*, 2903−2907.